

pubs.acs.org/JPCC Article

Site-Selective Ion Intercalation Controls Spectral Response in **Electrochromic Hexagonal Tungsten Oxide Nanocrystals**

Published as part of The Journal of Physical Chemistry virtual special issue "Horst Weller Festschrift".

Benjamin Z. Zydlewski, Hsin-Che Lu, Hugo Celio, and Delia J. Milliron*



Cite This: J. Phys. Chem. C 2022, 126, 14537-14546



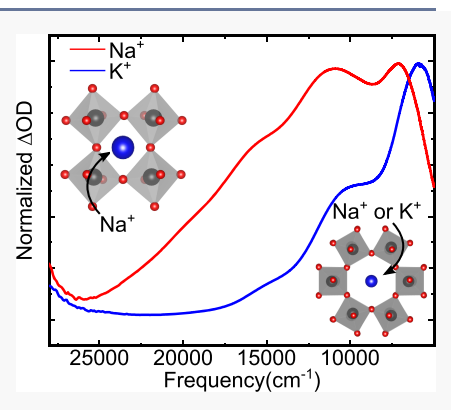
ACCESS

III Metrics & More

Article Recommendations

Supporting Information

ABSTRACT: The electrochromism of tungsten oxide occurs through electrochemical reduction, providing active solar control to smart windows, but control over the spectral response is limited and largely empirical. To determine how specific chemical changes result in the optical absorption processes responsible for coloration, we pair structurally well-defined electrochromic nanocrystals (NCs) with cations of varying ionic radii to limit intercalation into specific crystallographic sites. The localized surface plasmon absorption of hexagonal cesium-doped tungsten oxide (Cs:WO₃) NCs is enhanced, and new absorption features appear, depending on how the cations intercalate into various interstitial voids. These differences were rationalized using X-ray photoelectron and Raman spectroscopies to reveal the chemical and structural changes leading to the observed variations in the electrochemically induced absorption spectra. Smaller cations, Na⁺ and Li⁺, can access additional interstitial sites, leading to a secondary, polaronic mechanism of electrochromism, accounting for enhanced visible light absorption.



INTRODUCTION

Electrochromic materials that can dynamically modulate the transmittance of infrared and visible light independently are essential for the development of energy-saving window technologies. Electrochemical charging and discharging modulate the optical properties in response to a potential bias, resulting in reversible coloring and bleaching. By controlling the transmittance of solar radiation, we can limit unwanted heating and regulate natural lighting, improving building energy efficiency.²⁻⁴ Both amorphous and crystalline forms of tungsten oxide absorb visible and near-infrared light when electrochemically reduced, making it one of the most heavily studied materials for electrochromic window technologies. More recent research has shown that nanocrystalline forms of tungsten oxide demonstrate localized surface plasmon resonance (LSPR), allowing selective optical modulation in the near-infrared.^{7,8} LSPR is a property of conductive nanoparticles where the free charge carriers oscillate collectively in resonance with the electric field of incident light, leading to strong absorption. This absorption occurs throughout the infrared for various conductive metal oxides, making it ideal for controlling the transmittance of infrared light in solar radiation.9

LSPR can be modulated electrochemically through oxidation or reduction, which varies the population of free charge carriers that contribute to light absorption. Electrochemical modulation of LSPR has been described as due to purely capacitive charging, which is a surface property where charge is stored in the electrical double layer at the interface between the electrolyte and electrode surface. The modulation of the LSPR of Sb:SnO₂ and Sn:In₂O₃ NCs has been shown to be mostly independent of the electrolyte cation used, with only small differences between electrolytes containing lithium and tetrabutylammonium (TBA+) cations. Differences in the spectral response arising at more strongly reducing potentials have been ascribed to the irreversible intercalation of lithium and the reduction of either Sb or Sn. 10,11 The crystal structures of these materials do not contain easily accessible interstitial voids or channels for cations to diffuse through reversibly during electrochemical cycling. However, plasmonic tungsten oxide NCs do contain cation-accessible interstitial sites. Tungsten oxide exists in various phases, all containing different arrangements of WO₆ octahedra. The various crystal phases of tungsten oxide allow for cation intercalation into the interstitial voids between the tungsten octahedra, but the impact ion intercalation has on the LSPR of tungsten oxide NCs is not well understood.

The electrochromism of thin films of tungsten oxide has been studied extensively, and the change in the optical properties upon electrochemical reduction has been attributed

Received: April 25, 2022 Revised: August 8, 2022 Published: August 23, 2022





to the formation of polaronic states or an increased concentration of conduction electrons. 6,12 Polarons are electronic states in which charge carrier localization is associated with a local lattice distortion. These localized states can hop between neighboring sites of differing valence through the absorption of a photon. The energy required for the charge-transfer between neighboring tungsten octahedra leads to the visible absorption of reduced tungsten oxides. Localized states can form near defect sites such as oxygen vacancies or interstitial cations formed during intercalation. For materials such as tungsten oxide with multiple different interstitial sites that cations can occupy, it is not well understood if specific sites favor charge localization or if their occupation introduces shallow donors that contribute free charge carriers to the conduction band. Distinguishing between optical absorption due to polaronic states and free carrier effects such as the LSPR we observe in tungsten oxide NCs is difficult due to the similar frequency ranges these processes occur in, but we investigate the extent of charge localization to provide an indication of which mechanism is contributing to the decreased transmittance of tungsten oxide NCs during electrochemical reduction.

Specifically, we look to better understand the electrochromism of tungsten oxide by comparing the electrochromism of hexagonal cesium-doped tungsten oxide NCs (Cs:WO3 NCs) reduced in electrolytes containing cations of varying ionic radius. The hexagonal phase of tungsten oxide has been shown to be difficult to synthesize without the incorporation of a stabilizing cation (Cs+, Rb+, NH4+) that occupies the hexagonal channels due to more favorable formation of the monoclinic or tetragonal phases.¹³ The hexagonal Cs_xWO₃ phase has been shown to be stable for compositions between x = 0.15 and x = 0.33. The incorporated Cs⁺ acts as an interstitial dopant, being compensated by electrons in the conduction band. 15,16 The Cs⁺ doping leads to the LSPR absorption observed in nanocrystalline forms of this material due to the high population of free charge carriers. The absorption band also occurs in the near-infrared (NIR), making LSPR modulation in Cs:WO₃ NCs attractive for NIR-selective electrochromic windows. The hexagonal crystal structure contains several different interstitial channels that allow for the reversible intercalation of cations such as Li⁺ or Na⁺, but it is not well understood how intercalation into different sites in the material impacts the LSPR absorption. It has been previously shown that the coloration efficiency of monoclinic WO_{2.72} NCs could be increased by selective intercalation into larger interstitial sites using sodium-based electrolytes compared to electrolytes based on smaller lithium cations. 17 Sodium ions were inhibited from occupying the small trigonal sites, which contribute only weakly to the optical response, improving the coloration efficiency. Similar results have been shown for hexagonal tungsten oxide nanorods, which showed variations in the amount of achievable coloration based on different surface faceting of the particles, varying the amount of accessible sites for lithium intercalation.¹⁸ Here, in Cs:WO₃ NCs we reveal that site-selective occupation of interstitial sites based on differential cation size can not only tune the magnitude of the coloration but also give rise to dramatically different spectral signatures. We assign these distinct spectral responses to either plasmonic or polaronic absorption, based on the extent of charge localization.

EXPERIMENTAL SECTION

Cs:WO₃ NCs were synthesized using standard Schlenk line techniques under an inert atmosphere, as previously described. 7,19,20 The synthesis involves the injection of tungsten oleate into a hot solution of cesium oleate at 300 °C. The two metal oleates were prepared separately by the reaction of tungsten(IV) chloride or cesium chloride with oleic acid. After injection, the reaction was allowed to proceed for 10 min, and then the dark blue mixture was cooled quickly to stop the reaction. The NCs were purified after synthesis by precipitating them out of the reaction mixture with isopropanol acting as an antisolvent. The NCs were centrifuged to separate the precipitated NC product, and the supernatant was discarded. The mixture was redispersed in toluene and washed again by addition of antisolvent and subsequent centrifugation. The final NC colloid was prepared by redispersing the product in hexane with an approximate concentration of 20 mg/mL. The colloidal NC dispersion was concentrated to 50 mg/mL, and 30 μ L were used to spin-coat thin films on conductive, tin-doped indium oxide (ITO)coated glass substrates at 1500 rpm. These films were then annealed in a furnace at 400 °C under air to remove the oleic acid ligands that coat the surface of the NCs to improve film conductivity. Film thickness was measured to be 35 nm using an Alpha-Step D-500 stylus profilometer. No structural change was observed using X-ray diffraction (XRD) in NC powders annealed under the same conditions, indicating the hexagonal crystal structural and NC morphology are not impacted by the annealing process. These NC thin films were then used as electrodes to study their electrochromic properties.

The electrochromic responses of the NC films were investigated using in situ spectroelectrochemistry. An NC film served as the working electrode in an optically transparent electrochemical cell controlled by a Biologic VMP3 potentiostat, which was placed between fiber optic cables coupled to an ASD Quality Spec Pro visible-near-infrared spectrometer. A schematic of the spectroelectrochemical cell is shown in Scheme S1. For lithium electrolyte-based experiments, a lithium foil was used as both the counter and reference electrodes. For measurements utilizing other electrolyte cations, a silver/silver cation reference electrode and a platinum foil counter electrode were used. All electrolytes were prepared in propylene carbonate at 0.1 M concentration of metal hexafluorophosphate salt of formula XPF6, where X is Li+, Na+, K+, or TBA+. All electrochemical experiments were carried out in an argon glovebox to avoid water or oxygen contamination.

The relevant electrochemical potential window for the reversible color change of Cs:WO₃ NCs was determined by monitoring the change in transmittance as a function of the applied potential using chronoamperometry (Figures S1 and S2). The potential window and charge capacity found using chronoamperometry were used to determine the appropriate current density to achieve an approximate 1C charging rate of the NC films in each of the four electrolytes. Films were charged with a constant current, and absorbance spectra were taken at set time intervals, corresponding to known amounts of stored charge (Figures S3 and S4). The ratio of incremental changes in optical density (Δ OD) to stored charge determines the coloration efficiency. All absorbance measurements were taken in transmittance mode and backgrounded with a clean piece of ITO coated glass in the electrochemical cell filled with

electrolyte. The OD changes are then referenced to the fully transparent state.

XRD of the NC sample was done by precipitating a powder from a dispersion in hexane through the addition of excess isopropanol. The dried powder was mounted on a cryoloop with mineral oil for measurement. A Rigaku R-Axis Spider with a Cu K α source was used to collect the diffraction pattern. Crystal structure visualizations were created using VESTA.²¹

Scanning transmission electron microscopy (STEM) was used to image the NCs. A carbon-coated copper grid was coated with the NC sample by dropping 20 μ L of a 1 mg/mL dispersion in hexane. After drying overnight in a vacuum desiccator, the sample was imaged using a Hitachi S5500 microscope in STEM mode.

X-ray photoelectron spectroscopy (XPS) was used to assess changes in the electronic state of tungsten as the NC films were reduced. Films were prepared for XPS by electrochemically reducing them at a set potential for 10 min, followed by washing of the films with dimethyl carbonate to remove excess electrolyte. The potential used to reduce the films corresponds to the lowest potential used to reversibly color the films. Films were transferred from a glovebox to the XPS using an air-free capsule that mechanically couples to a semiautomatic interface on the XPS. This interface evacuates the capsule via differential pumping to prevent air exposure during the transition from high pressure to ultrahigh vacuum (patent 9945761).²² Preventing air exposure allowed for the transfer of the films to the XPS chamber without contamination or discharging due to contact with water or oxygen. The photoemission spectra of the films were measured using a Kratos X-ray Photoelectron Spectrometer – Axis Ultra DLD using an Al K α source.

Raman spectroscopy was performed using a Horiba LabRAM Aramis instrument using a 50× microscope objective and a 532 nm laser as the excitation source. NC dispersions were drop-cast on aluminum foil substrates. Electrochemically reduced samples were prepared in an Ar glovebox and transferred in a sealed LTS420 Linkam cell to measure the ex situ Raman spectra without exposing the samples to air or water.

■ RESULTS AND DISCUSSION

The hexagonal crystal structure of cesium-doped tungsten oxide leads to anisotropy in NC morphology (Figure 1a-c). The XRD pattern confirms that the NCs are the hexagonal phase of tungsten oxide (Figure 1d), and XPS confirms the presence of cesium in the material (Figure S5). The presence of these cations is crucial to stabilizing the otherwise metastable hexagonal crystal structure. 13 The cesium cations also act as interstitial dopants, with the excess charge of the cations being compensated by electrons in the conduction band of the material. Various alkali metal doped tungsten oxide phases, commonly known as tungsten bronzes, have been shown to be metallic conductors due to the high concentration of free electrons generated by the interstitial cations.¹⁶ When nanocrystalline materials with high charge carrier concentrations are illuminated, these electrons oscillate in resonance with the electric field of light, producing localized surface plasmon resonance. LSPR in conducting metal oxide NCs results in strong absorption of NIR light (Figure 2a). The LSPR of the dispersion of NCs shows two distinct peaks, which correspond to two unique plasmon modes, a result of the anisotropy in particle shape and electronic structure (effective mass and damping) between the two unique

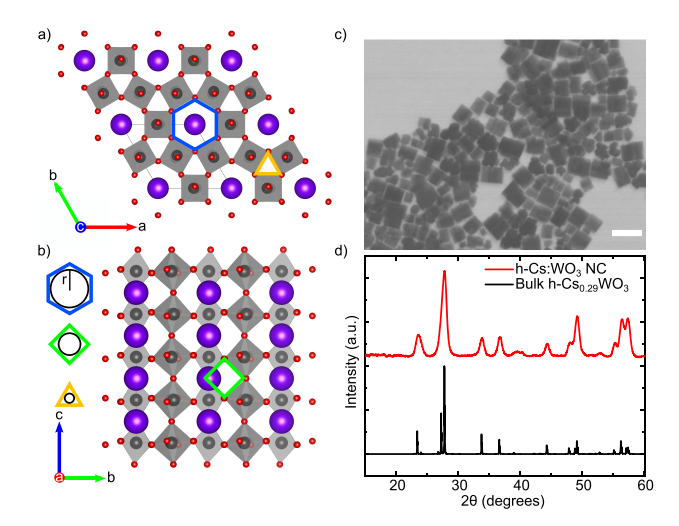


Figure 1. (a) Crystal structure of hexagonal $Cs_{0.29}WO_3$ viewed along c-axis. (b) Crystal structure of hexagonal $Cs_{0.29}WO_3$ viewed along the a-axis. The various interstitial channels are highlighted to show the varying size and location within the crystal structure. The gray, red, and purple spheres correspond to tungsten, oxygen, and cesium, respectively. Crystal structure visualizations were created using VESTA. (c) STEM image of Cs:WO₃ NCs. The scale bar represents 40 nm. (d) X-ray diffraction pattern of Cs:WO₃ NCs with reference pattern for bulk hexagonal $Cs_{0.29}WO_3$ (ICSD #56223).

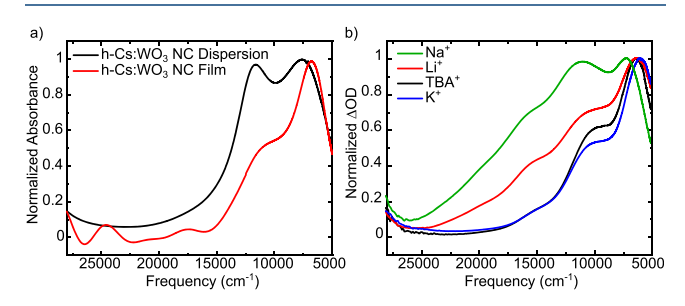


Figure 2. (a) UV–vis–NIR absorption spectra of a colloidal dispersion and film of h-Cs:WO $_3$ NCs. (b) Change in optical density of h-Cs:WO $_3$ NC films reduced in electrolytes consisting of 0.1 M XPF $_6$ (X = Na, Li, TBA, K) in propylene carbonate. The films were reduced to 7.4, 7.5, 3.3, and 1.9 mC/cm 2 for the films reduced in electrolytes containing Li $^+$, Na $^+$, K $^+$, and TBA $^+$, respectively. The capacities varied based on the electrolyte cation, but the spectra are normalized to show the difference in the spectral line shape.

crystallographic directions of the hexagonal crystal structure.^{7,19} The LSPR spectrum of the NCs broadens when they are deposited as a film due to plasmonic coupling between the NCs, but the bimodal structure is still apparent (Figure 2a). The oscillations at high frequencies (~25 000 and ~17 500 cm⁻¹) are the result of interference fringes due to the glass substrate and are not relevant to the analysis of the LSPR spectra. The NIR peak of the LSPR and wide band gap, in the UV, allows for high transparency in the visible region, with only the tail of the LSPR spilling over into the red edge of the visible, leading to the blue coloration of the NCs. After the removal of the surface-capping ligands by annealing in a furnace under air, the NC films can be reversibly electrochemically cycled. The oxidation in air bleaches the LSPR of the NC films, which can be colored through electrochemical reduction. Reduction induces an electrochromic response leading to increased absorption of visible and NIR light,

while recovering the transparent state upon electrochemical oxidation. The change in OD with electrochemical reduction varies depending on the electrolyte cation used to compensate the injected charge (Figure 2b). TBA+ electrolytes have been previously used to enforce a purely capacitive charging mechanism. 17 In our case, capacitive charging in a TBA+ electrolyte results in a modulation spectrum (ΔOD) that matches very closely to the LSPR of the pristine material. Comparing this response to the electrochromism due to intercalation of the smaller cations, we see significant differences in the spectral line shape.

The differences in spectral line shape between the samples reduced in each of the electrolytes suggest that there are different electrochromic mechanisms depending on which interstitial sites are occupied. Films reduced in Li⁺ and Na⁺ electrolytes show similar increased modulation in the visible region (12 500-25 000 cm⁻¹), which is absent in films reduced in K⁺ or TBA⁺ electrolytes. If the occupation of the various interstitial sites in the hexagonal crystal lattice contributed in the same way to the electrochromism, one would expect changes only in the magnitude of the Δ OD, but not in the line shape. The overall line shape of the Δ OD spectra of the films reduced in K⁺ or TBA⁺ electrolytes shows a similar shape to the LSPR spectrum of the NC film prior to annealing as shown in Figure 2a. This similarity suggests that the electrochromism in these films is the result of purely LSPR modulation. The LSPR modulation in other metal oxide NC systems is consistent with the results shown here, where there is minimal LSPR peak shift, but substantial LSPR intensity increase with electrochemical reduction. 10,23 The minimal LSPR peak shift is attributed to the filling of a depletion layer near the surface of the NCs, which results primarily in modulation of the LSPR active volume, but not the overall carrier concentration. A comparison between films reduced to the same extent in both Li⁺ and K⁺ electrolytes shows that it is not just a factor of the increased charge storage between the smaller and larger cations leading to the higher energy absorption (Figure S6). The Li⁺ intercalated film still shows enhanced modulation in the visible region when reduced to the same state of charge as a film intercalated with K⁺. The increased modulation in the visible region suggests that the intercalation of the smaller cations results in a secondary mechanism of electrochromism.

To understand how the intercalation of different sized cations influences the electrochromic spectral response, we must first consider the size of the interstitial sites in the hexagonal lattice. The hexagonal crystal structure has three interstitial voids that vary in size. The first are the large hexagonal channels that run along the c-axis of the crystal structure. The second are the smaller trigonal channels that run parallel to the c-axis as well. The last set of pathways ions can potentially diffuse through are the square channels that run orthogonal to the other two. To compare the approximate size of these different voids in the material, a circle was inscribed in the channel and the radius was used to compare the relative sizes of the different sites (Figure 1a and 1b). The approximate sizes are 236, 78, and 129 pm for the hexagonal, trigonal, and square sites, respectively. The ionic radii of the four cations used in this study are 60, 95, 133, and 494 pm for Li⁺, Na⁺, K⁺, and TBA+, respectively. 24 Comparing the relative sizes of the ionic radii to the sizes calculated for the different sites in the material, we expect larger cations to be inhibited from diffusing through certain sites. The ionic radius of the lithium cation is small enough that it is expected to be able to freely diffuse

through all the sites. The opposite can be said for TBA⁺. Its much larger size limits its ability to intercalate into the material at all, which restricts it to purely surface charging. Na⁺ is small enough that it is expected to be able to diffuse through the square and hexagonal channels, while K⁺ is only expected to be able to diffuse through the hexagonal channels. Based on this analysis and the observed electrochromism, it appears that the ability for Li⁺ and Na⁺ to diffuse through and occupy sites within the smaller square channels leads to a secondary mode of absorption during electrochemical reduction in addition to LSPR modulation which results from occupation of the hexagonal channels.

The optical properties of hexagonal cesium tungsten oxide that have been reported include both plasmonic and polaronic excitations, but it has not been shown that these two different mechanisms can be activated based on different electrochemical reduction pathways.²⁵ It has been hypothesized that the higher energy absorption, greater than approximately 12 500 cm⁻¹, is the result of polaron formation in the material. The slightly lower energy excitations that appear further in the NIR have been assigned to LSPR. 19 It has also been shown that varying amounts of cesium occupation in the hexagonal crystal structure primarily impacts the extinction of the lower energy optical transitions, suggesting the cesium primarily contributes free electrons to the conduction band, amplifying the plasmonic absorption. Theoretical calculations of hexagonal tungsten oxide with varying occupation of the hexagonal channels with alkali metal cations is consistent with our theory. The calculations indicate that cations occupying the hexagonal sites donate free electrons; in NCs these electrons would result in LSPR, as we observed. 15 Machida et al. reported that varying oxygen content led to variation in the extinction of the material at higher energy. They hypothesized that the higher energy extinction was due to the increased oxygen vacancy concentration leading to an increased amount of polaronic states. 25,26 This idea of different electronic states, associated with distinct charge compensating defects, leading to different optical absorption processes can correspondingly rationalize the cation-dependent electrochromic modulation spectra we observe.

To investigate the differences in the electronic state of tungsten during electrochemical reduction, we turned to XPS. The electrochromism occurs due to the injection of electrons into the material, but what electronic states result and how these contribute to the optical response of hexagonal tungsten oxide are debated in the literature. 15,27 For plasmonic electrochromism, these electrons occupy the conduction band of the material, which increases the electron concentration or volume of LSPR active material, leading to increased LSPR extinction. For polaronic electrochromism, the electrons are localized on WO₆ octahedra by distorting the surrounding crystal lattice. The optical response is the result of the hopping of these electrons to nearby octahedra of differing valence state through the absorption of a photon. The electrochromic mechanism is thus correlated with the degree of charge localization, which was probed using XPS to determine if the electronic states depend on the intercalation sites occupied by the cation during reduction.

Using XPS to compare the changes in electronic state of tungsten with electrochemical reduction, we identified some key differences between the films reduced in different electrolytes. The W 4f photoemission spectra for a pristine film and films reduced in electrolytes containing Na⁺ or K⁺ are

shown in Figure 3 with the fitting parameters reported in Table 1. The W 4f photoemission spectra for films reduced in TBA⁺

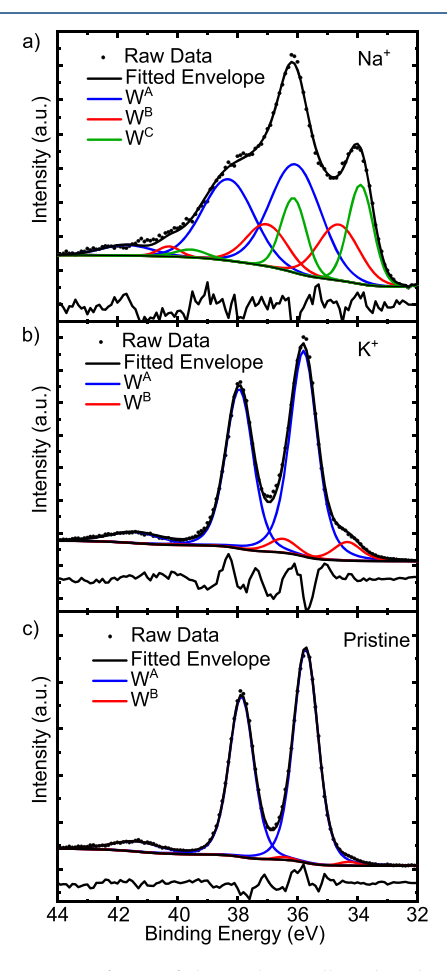


Figure 3. Ex situ W 4f XPS of electrochemically reduced Cs:WO $_3$ NC films. (a) NC film reduced in Na $^+$ electrolyte. (b) NC film reduced in K $^+$ electrolyte. (c) Pristine NC film prior to any electrochemistry. The spectra show 2–3 distinct doublets representing electronic states. They are labeled from highest to lowest binding energy W A , W B , and W C , respectively.

and Li⁺ are shown in Figures S7 and S8. Mirroring the similarities between the optical spectra of the samples, the films reduced in K⁺ and TBA⁺ electrolytes show very similar W 4f spectra. Likewise, the other two films reduced in Li⁺ or Na⁺ electrolytes have similar W 4f spectra. Compared to a pristine NC film, the films reduced in Li⁺ or Na⁺ electrolytes show a much more significant change in the W 4f photoemission spectra, with much greater intensity at lower binding energy. Tungsten 4f photoemission spectra consist of spin—orbit doublets with an energy splitting of 2.1–2.2 eV. ^{28,29} These

parameters were used to fit the photoemission spectra to multiple doublet components, indicating the presence of different tungsten electronic states. After fitting the spectra to deconvolute different W electronic states, the Li $^{\rm +}$ and Na $^{\rm +}$ films show a lower binding energy doublet in addition to the two doublets observed in the spectra of films reduced in K $^{\rm +}$ and TBA $^{\rm +}$ electrolytes. Based on the W 4f photoemission spectra there is a significantly larger amount of reduced tungsten for the Li $^{\rm +}$ and Na $^{\rm +}$ intercalated tungsten oxide.

The interpretation of multipeak structures in the photoemission spectra of metal oxides is actively debated. 30-35 The first interpretation is that each component represents localized valence states, with a distribution of different states throughout the tungsten oxide octahedral network. The second interpretation is that the multiple components are derived from final-state effects due to interactions of the core-holes generated during photoemission with the valence electrons. Both interpretations have merit and reliable methods of differentiating between these two effects are not well established. Based on the photoemission spectra, there are two possible interpretations to the differences in the electronic state of tungsten in each sample and how it relates to the mechanisms for electrochromism.

The W 4f photoemission spectra of NC films that have been electrochemically charged show significant populations of tungsten in more reduced states. All NC films show a doublet (W^B) of varying intensity 1.4–1.5 eV lower in binding energy than the highest energy W 4f doublet (W^A). In addition to W^B , films reduced in Li⁺ and Na⁺ electrolytes show another doublet (W^C) 2.2 eV lower in binding energy than W^A. The XP spectra of these films also show higher intensity in both low binding energy doublets, indicating a much larger population of both reduced tungsten states compared to the other samples. The more dominant presence of reduced tungsten species could be interpreted as a greater amount of charge stored on tungsten cations in the material. Differing amounts of charge localization helps explain the differences in the electrochromic line shapes between samples. Greater charge localization as a function of lithium-ion intercalation has been used to explain increased visible light electrochromism in niobium oxide NCs as well. 36 This supports our hypothesis that the visible light absorption of Cs:WO3 NCs comes from the localization of charge during the double injection of electrons and cations into the material. The small increase in reduced tungsten species for films reduced in K⁺ and TBA⁺ electrolytes could either be due to a small amount of the reduction of surface tungsten atoms or be the result of final-state effects that become more influential at higher carrier concentrations.

The presence of multiple components in photoemission spectra of metallically conductive oxides has also been attributed to final-state effects, which result from interactions

Table 1. XPS Fitting Parameters for Films Electrochemically Reduced in Various Conditions

Reduction Condition	$W^A 4f_{7/2} BE (eV)^a$	W^A $4f_{7/2}$ fwhm $(eV)^b$	W^B $4f_{7/2}$ BE $(eV)^a$	W^B $4f_{7/2}$ fwhm $(eV)^b$	W^C $4f_{7/2}$ BE $(eV)^a$	W^C $4f_{7/2}$ fwhm $(eV)^b$
Pristine	35.7	1.0	34.3	0.7	_	_
TBA^+	35.9	1.3	34.4	1.0	_	_
K ⁺	35.8	1.1	34.3	1.1	_	_
Na ⁺	36.1	2.0	34.6	1.6	33.9	1.0
Li ⁺	36.1	1.7	34.6	1.0	33.9	0.7

^aThe W $4f_{5/2}$ peaks were constrained to 2.14 eV higher than the W $4f_{7/2}$ components based on the splitting observed in the pristine sample, which is consistent with literature values. ⁴⁶ ^bThe fwhm for the W $4f_{5/2}$ component was constrained to be equal to the fwhm of the W $4f_{7/2}$ component.

between the core-holes created during photoemission and the electrons near the Fermi level. 34,37,38 Final state effects lead to two different components in the photoemission spectra, the higher binding energy unscreened component and the lower binding energy screened component. The screened component results from interactions with the electrons in the conduction band, resulting in a slightly lower binding energy. The splitting has been attributed to the screening of the photoelectron through the excitation of a plasma oscillation of the conduction electrons, with the energy difference corresponding to the bulk plasma energy. 31,33,39 The consistent energy difference between component W^A and W^B of 1.4-1.5 eV is similar to the bulk plasmon energies measured by electron energy loss spectroscopy for metallically conductive oxides such as MoO₂, WO2, and NaxWO3, which also show similar multicomponent Mo 3d and W 4f PES spectra, respectively. 40,41 It has also been shown that the relative intensity of the screened final state increases in intensity relative to the unscreened component with increasing carrier concentration in other doped metal oxides, which is also consistent with the increased intensity of W^B relative to W^A when comparing the pristine and reduced samples. 42 Considering the impact of final state effects, the individual spin-orbit doublets in Figure 3 are not a result of isolated, reduced tungsten species within the material, but a result of the increased concentration of conduction band electrons occupying the tungsten 5d-derived band. Consistent with this accumulation of charge, there is increased intensity near the Fermi level in the valence band photoemission spectra following reduction (Figure 4).

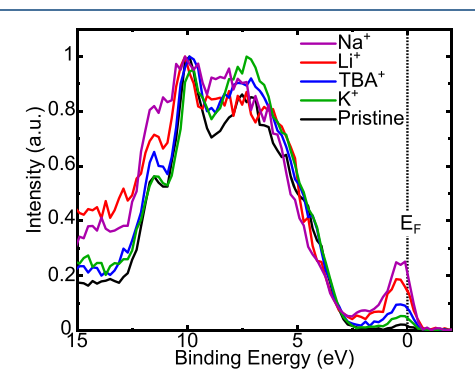


Figure 4. Valence band photoemission spectra of Cs:WO₃ NC films reduced in electrolytes containing various cations. The spectra are normalized to the intensity of the valence band.

The relatively low intensity of the screened component compared to the unscreened component could be explained by the presence of a depletion layer devoid of free charge carriers near the oxide surface, which for other metal oxides has been shown to be of similar nanometer length scales as the probe depth of XPS. 43-⁴⁵ The filling of a depletion layer near the NC surface explains the relative increase in intensity of the small band near the Fermi level compared to the valence band as the material is reduced (Figure 4). This small band increases in intensity, but the valence band does not noticeably shift in energy, indicating that the Fermi level is not increasing with electrochemical charging, while the depletion layer near the surface is being reduced in size. The narrowing of the depletion region places more weakly bound conduction electrons within the photoelectron escape depth, resulting in the increased intensity we observe.

The filling of a depletion layer has also been used to explain the limited shift in the LSPR peak position of metal oxide NCs, including Cs:WO₃ NCs, upon chemical or electrochemical reduction. The LSPR intensity increases following electron transfer to the NCs with little to no peak shifts, which is unexpected based on the relationship between the plasma frequency and carrier concentration. The modulation of LSPR in Cs:WO₃ NCs has been modeled previously as the filling of a shell depleted of conduction electrons near the surface of the material, both when chemically reduced with hydrazine and when electrochemically reduced in nonaqueous electrolytes. The electronic changes we observed using XPS and the changes in the optical properties are consistent with the filling of a depletion layer near the NC surface during electrochemically reduction.

Final-state effects account for the increase in intensity of W^B in the photoemission spectra of the reduced films compared to the pristine material, which is consistent with the increased LSPR intensity in the UV-vis-NIR spectra with reduction. Accounting for W^A and W^B as unscreened and screened final states due to the conduction band electrons, we assign W^C as a more strongly localized state resulting from cation intercalation. Most likely, the lowest binding energy W^C corresponds to a polaronic state that involves a lattice distortion and localization of the electronic charge, which would change the local electronic environment and shift the W 4f binding energy. When comparing the photoemission peaks, we note that W^C is much narrower compared to the other two components in Figure 3a, indicating a longer lifetime of that state, which is expected for a more localized state (Table 1). Significant charge localization is also expected to be correlated with structural rearrangements of the tungsten octahedra.

In addition to the changes in the electronic properties of hexagonal tungsten oxide with electrochemical reduction, we monitored structural changes using Raman spectroscopy (Figure 5). Raman spectroscopy probes the entire volume of

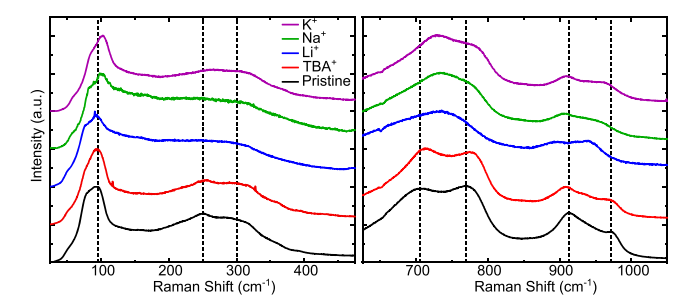


Figure 5. Raman spectra from (a) $0-500~\rm cm^{-1}$ and (b) $600-1100~\rm cm^{-1}$ of h-Cs:WO $_3$ NC films reduced in electrolytes of 0.1 M XPF $_6$ (X = Na, Li, TBA, K) in propylene carbonate along with the pristine material prior to electrochemical reduction.

material, providing insight into bulk structural changes that occur due to ion intercalation and helping resolve uncertainties owing to the surface sensitive nature of XPS. The pristine NCs prior to any electrochemical reduction show multiple Raman modes between 50 and 150 cm⁻¹, 200–350 cm⁻¹, 650–800 cm⁻¹, and 850–1000 cm⁻¹. These modes correspond to lattice modes, δ (O–W–O), ν (O–W–O), and ν (W=O), respectively. The most prominent differences between the reduced and pristine films occur in the ν (O–W–O) modes located between 650 and 800 cm⁻¹. For the Li⁺ intercalated film, there are significant changes to the peaks corresponding

to this mode, with the two peak structure present in the pristine sample merging into one broad peak. The blue shift of the lower frequency peak and red shift of the higher frequency peak are consistent with changes in the lattice parameters during the intercalation of cations, with the c-axis shortening and the a-axis lengthening.²⁷ The two peak structure has been assigned as $\nu(O-W-O)$ modes in the two crystallographic directions, with the lower frequency peak corresponding to the c-axis. The merging of these two peaks is most easily seen in the Li⁺ intercalated film, but similar shifts are shown for the Na⁺ intercalated film. The results for the K⁺ intercalated film are less clear, with a significant blue shift of the lower frequency peak, but a much less significant shift in the higher frequency one. The reduction of the material in a TBA+ electrolyte does not impact the two-peak structure in this region, which is consistent with our interpretation that this structural change is the result of cation intercalation.

In addition to the changes in the $\nu(O-W-O)$ modes, the lower frequency Raman peak corresponding to the δ (O-W-O) mode decreases in intensity and broadens. The film reduced in TBA+ electrolyte does not show as significant broadening, furthering our hypothesis that the structural changes are the result of cation intercalation. The last major difference is in the higher frequency peaks related to the ν (W=O) modes. This double bond stretching mode has been assigned to terminal tungsten oxygen bonds, occurring both for tungsten ions near oxygen vacancies and due to surface termination of the tungsten octahedra. 48,49 Both of these structural motifs are plausible contributors for our samples, considering the high surface area of nanocrystalline materials and the prevalence of oxygen deficiencies in various tungsten oxide phases. The $\nu(W=O)$ modes shift to lower frequency in all reduced samples relative to the pristine sample, which could be related to the reduction of tungsten cations in the material. Reduction of tungsten to lower oxidation states causes an increase in W-O bond length and softening of that bond, due to the lower charge of the tungsten. The structural changes observed for Li⁺ and Na⁺ intercalated films are consistent with our hypothesis that the insertion of these cations into the material results in more significant charge localization associated with polaronic states.

We hypothesize that the electrolyte-dependent differences in electrochromic properties of hexagonal cesium tungsten oxide are the result of different electronic states that result from the intercalation sites occupied during electrochemical reduction. Based on the optical and XPS data, the intercalation of potassium, which is expected to be limited to the hexagonal tunnels in the material, coincides with the injection of free electrons. These electrons expand the plasmonic volume within each NC, resulting in the increased extinction of the LSPR, a response which is almost identical to that for films reduced in an electrolyte containing TBA+. Charging with TBA+-based electrolytes is capacitive and gives rise to an increased population of free electrons. The spectral change in films reduced in these two electrolytes is consistent with a purely plasmonic modulation of the extinction. The optical response to intercalation of the two smaller cations deviates from the LSPR line shape, which we ascribe to the formation of polaronic states due to intercalation into interstitial sites inaccessible to larger cations. We hypothesize that the ability of these smaller cations to diffuse through the square channels and occupy sites within these voids leads to visible light electrochromism. The similar capacities observed in lithium

and sodium electrolytes point to the same type of intercalation sites being accessible. The observed capacities of 7.4 and 7.5 mC/cm² for Li⁺ and Na⁺ electrolytes were used to calculate the relative amount of intercalated cation to the amount of tungsten oxide. The mass loading of tungsten was calculated based on the film thickness, area, density, and porosity. The porosity of similarly shaped Cs:WO₃ NCs was previously measured to be 14.5%, which was used in our calculation. Based on this analysis, the capacities in Li⁺ and Na⁺ electrolytes correspond to an approximate 1:1 stoichiometry of intercalated cation to tungsten. Even with the expected high surface area of the nanocrystalline electrode, we would expect most of this charge to correspond to insertion of Li⁺ or Na⁺ into the material. The capacities in K⁺ and TBA⁺ electrolytes of 3.3 and 1.9 mC/cm² are significantly less, supporting our hypothesis that these two cations are unable to access the smaller intercalation sites available to Li⁺ and Na⁺.

The coloration efficiency, which is the amount of optical density change per unit of injected charge, is also dependent on the electrolyte cation used. The coloration efficiency at longer wavelengths in the NIR is similar across all electrolytes, with only lithium showing a slightly higher coloration efficiency, which could be related to its expected ability to diffuse through the small trigonal channels in the material or the ability to more readily diffuse around cesium cations blocking pathways through the hexagonal channels.⁷ In the visible range, the coloration efficiency is substantially different between the smaller cations (Li⁺ and Na⁺) and the larger cations (K⁺ and TBA⁺). The smaller cations have coloration efficiencies between 40 and 50 cm²/C, while the larger cations have coloration efficiencies between 12 and 15 cm²/C (Table S1). The higher coloration efficiency in the visible range for Li⁺ and Na+ is consistent with our hypothesis that polaronic electrochromism leads to enhanced visible light modulation due to the intercalation of these smaller cations. Prior literature has suggested that even though Li⁺ has a smaller ionic radius than the spacing of the trigonal channels in the crystal structure, it is still not able to diffuse through these smaller channels. 50,51 Although, prior work done by Heo et al. suggested that the ability for Li⁺ to more freely diffuse through these smaller channels allowed for the increased capacity observed in Li⁺ electrolytes compared to Na⁺ ones for monoclinic tungsten oxide nanorods. Na+ is believed to be unable to diffuse through these trigonal sites due to the larger size of the cation. Due to the similar observed capacities of the material in these two electrolytes, we believe that the ability for these two cations to diffuse through the square channels in the material leads to the increased capacity, with the trigonal channels being too small to allow for ion diffusion for the hexagonal crystal structure.

The ability for these smaller cations to access more sites in the material suggests an explanation for the differing electrochromic properties for NC films reduced in these electrolytes. The occupation of these sites leads to an increase in the lowest binding energy W 4f peak seen by XPS, corresponding to a more reduced state of tungsten. The more reduced state then contributes to the higher energy optical transitions observed in the UV-vis-NIR spectra. This understanding illustrates that selecting cations for intercalation into specific interstitial sites is a viable design strategy to tune the spectral response of electrochromic materials. This approach can be used in combination with tuning the morphology of NCs to control the spectral line shape of the

electrochromism to tailor it to solar radiation, customize the optical tint, and better optimize spectrally selective NIR blocking smart windows to enable for increased building energy efficiency.

CONCLUSION

The mechanisms for electrochromism of various phases and morphologies of tungsten oxide have been heavily debated in the past several decades, but these results demonstrate that multiple different mechanisms may be operative depending on the interaction between intercalating cations and the electronic states and crystal lattice. The presence of different spectral line shapes for films reduced in Li⁺ and Na⁺ electrolytes suggests that, in addition to the increase in free electrons, some portion of the injected electrons localize. These localized electrons on tungsten cations lead to a higher energy optical absorption feature due to polaronic hopping, or charge transfer between different tungsten species in the material. The presence of localized electrons is evidenced by the increase in lower binding energy components in the W 4f photoemission spectra for these films. Due to the surface sensitivity of XPS, follow-up experiments probing the role of particle size could help provide more insight into the impact of capacitive versus bulk ion insertion processes. Complementary experiments to probe the overall change in tungsten oxidation state (e.g., by near-edge X-ray absorption spectroscopy) would help validate these connections between the reduction conditions, the electronic state of the material, and the electrochromic spectral response.⁵²

The distinct spectral response based on the electrolyte cation used opens new possibilities for tuning the spectral selectivity of smart window devices to overlap with the different regions of solar radiation. This strategy can be further used to understand and control the electrochromic properties of other intercalation-based materials that have multiple different sites for cation intercalation.³⁶ By using cations that limit intercalation into only select sites, we have shown that we can improve spectral selectivity for NIR light, while still maintaining high transparency in the visible region. This is enabling for smart window technologies that allow for selective blocking of NIR radiation, which leads to excess heat, while still maintaining high transparency for visible light to reduce lighting costs.⁴

ASSOCIATED CONTENT

Supporting Information

The Supporting Information is available free of charge at https://pubs.acs.org/doi/10.1021/acs.jpcc.2c02865.

Electrochemical data for chronoamperometry and chronopotentiometry experiments; UV—vis—NIR transmittance spectra as a function of applied potential; Change in optical density as a function of stored charge for NC films reduced in 4 different electrolyte conditions; W 4f XPS of electrochemically reduced NC films in Li⁺ and TBA⁺ electrolytes; Coloration Efficiency for visible and NIR wavelengths; Cs 3d and W 4f XPS for oxidized and pristine NC films; Absorbance spectra of NC films reduced to the same extent of stored charge in Li⁺ and K⁺ electrolytes; Schematic of spectroelectrochemical cell (PDF)

AUTHOR INFORMATION

Corresponding Author

Delia J. Milliron — Department of Chemistry, The University of Texas at Austin, Austin, Texas 78712, United States; McKetta Department of Chemical Engineering, The University of Texas at Austin, Austin, Texas 78712, United States; orcid.org/0000-0002-8737-451X; Email: milliron@che.utexas.edu

Authors

Benjamin Z. Zydlewski – Department of Chemistry, The University of Texas at Austin, Austin, Texas 78712, United States; occid.org/0000-0001-5591-1731

Hsin-Che Lu — McKetta Department of Chemical Engineering, The University of Texas at Austin, Austin, Texas 78712, United States; orcid.org/0000-0001-5673-2647

Hugo Celio – Texas Materials Institute, The University of Texas at Austin, Austin, Texas 78712, United States

Complete contact information is available at: https://pubs.acs.org/10.1021/acs.jpcc.2c02865

Notes

The authors declare the following competing financial interest(s): Delia J. Milliron has a financial interest in Heliotrope Technologies, a company pursuing commercial development of electrochromic devices.

ACKNOWLEDGMENTS

The authors acknowledge support from Companhia Brasileira de Metalurgia e Mineração (CBMM), the National Science Foundation (CHE-1905263), and the Welch Foundation (F-1848).

REFERENCES

- (1) Wu, W.; Wang, M.; Ma, J.; Cao, Y.; Deng, Y. Electrochromic Metal Oxides: Recent Progress and Prospect. *Adv. Electron. Mater.* **2018**, *4* (8), 1800185.
- (2) Granqvist, C. G.; Arvizu, M. A.; Bayrak Pehlivan, İ.; Qu, H.-Y.; Wen, R.-T.; Niklasson, G. A. Electrochromic Materials and Devices for Energy Efficiency and Human Comfort in Buildings: A Critical Review. *Electrochim. Acta* **2018**, 259, 1170–1182.
- (3) Tällberg, R.; Jelle, B. P.; Loonen, R.; Gao, T.; Hamdy, M. Comparison of the Energy Saving Potential of Adaptive and Controllable Smart Windows: A State-of-the-Art Review and Simulation Studies of Thermochromic, Photochromic and Electrochromic Technologies. Sol. Energy Mater. Sol. Cells 2019, 200, 109828.
- (4) DeForest, N.; Shehabi, A.; O'Donnell, J.; Garcia, G.; Greenblatt, J.; Lee, E. S.; Selkowitz, S.; Milliron, D. J. United States Energy and CO2 Savings Potential from Deployment of Near-Infrared Electrochromic Window Glazings. *Build. Environ* **2015**, *89*, 107–117.
- (5) Berggren, L.; Jonsson, J. C.; Niklasson, G. A. Optical Absorption in Lithiated Tungsten Oxide Thin Films: Experiment and Theory. *J. Appl. Phys.* **2007**, *102* (8), 083538.
- (6) Larsson, A.-L.; Sernelius, B. E.; Niklasson, G. A. Optical Absorption of Li-Intercalated Polycrystalline Tungsten Oxide Films: Comparison to Large Polaron Theory. *Solid State Ion* **2003**, *165* (1), 35–41.
- (7) Heo, S.; Cho, S. H.; Dahlman, C. J.; Agrawal, A.; Milliron, D. J. Influence of Crystalline and Shape Anisotropy on Electrochromic Modulation in Doped Semiconductor Nanocrystals. *ACS Energy Lett.* **2020**, *5* (8), 2662–2670.
- (8) Heo, S.; Kim, J.; Ong, G. K.; Milliron, D. J. Template-Free Mesoporous Electrochromic Films on Flexible Substrates from Tungsten Oxide Nanorods. *Nano Lett.* **2017**, *17* (9), 5756–5761.

- (9) Agrawal, A.; Cho, S. H.; Zandi, O.; Ghosh, S.; Johns, R. W.; Milliron, D. J. Localized Surface Plasmon Resonance in Semi-conductor Nanocrystals. *Chem. Rev.* **2018**, *118* (6), 3121–3207.
- (10) zum Felde, U.; Haase, M.; Weller, H. Electrochromism of Highly Doped Nanocrystalline SnO₂:Sb. *J. Phys. Chem. B* **2000**, *104* (40), 9388–9395.
- (11) Garcia, G.; Buonsanti, R.; Llordes, A.; Runnerstrom, E. L.; Bergerud, A.; Milliron, D. J. Near-Infrared Spectrally Selective Plasmonic Electrochromic Thin Films. *Adv. Opt. Mater.* **2013**, *1* (3), 215–220.
- (12) Svensson, J. S. E. M.; Granqvist, C. G. Modulated Transmittance and Reflectance in Crystalline Electrochromic WO₃ Films: Theoretical Limits. *Appl. Phys. Lett.* **1984**, *45* (8), 828–830.
- (13) Szilágyi, I. M.; Madarász, J.; Pokol, G.; Király, P.; Tárkányi, G.; Saukko, S.; Mizsei, J.; Tóth, A. L.; Szabó, A.; Varga-Josepovits, K. Stability and Controlled Composition of Hexagonal WO₃. *Chem. Mater.* **2008**, *20* (12), 4116–4125.
- (14) Adachi, K.; Asahi, T. Activation of Plasmons and Polarons in Solar Control Cesium Tungsten Bronze and Reduced Tungsten Oxide Nanoparticles. J. Mater. Res. 2012, 27 (6), 965–970.
- (15) Lee, Y.; Lee, T.; Jang, W.; Soon, A. Unraveling the Intercalation Chemistry of Hexagonal Tungsten Bronze and Its Optical Responses. *Chem. Mater.* **2016**, 28 (13), 4528–4535.
- (16) Hussain, A.; Gruehn, R.; Ruscher, C. H. Crystal Growth of Alkali Metal Tungsten Bronzes M_xWO_3 (M = K, Rb, Cs), and Their Optical Properties. *J. Alloys Compd.* **1997**, 246, 51–61.
- (17) Heo, S.; Dahlman, C. J.; Staller, C. M.; Jiang, T.; Dolocan, A.; Korgel, B. A.; Milliron, D. J. Enhanced Coloration Efficiency of Electrochromic Tungsten Oxide Nanorods by Site Selective Occupation of Sodium Ions. *Nano Lett.* **2020**, *20* (3), 2072–2079.
- (18) Evans, R. C.; Austin, R.; Miller, R. C.; Preston, A.; Nilsson, Z. N.; Ma, K.; Sambur, J. B. Surface-Facet-Dependent Electrochromic Properties of WO3 Nanorod Thin Films: Implications for Smart Windows. *ACS Appl. Nano Mater.* **2021**, *4* (4), 3750–3759.
- (19) Kim, J.; Agrawal, A.; Krieg, F.; Bergerud, A.; Milliron, D. J. The Interplay of Shape and Crystalline Anisotropies in Plasmonic Semiconductor Nanocrystals. *Nano Lett.* **2016**, *16* (6), 3879–3884.
- (20) Mattox, T. M.; Bergerud, A.; Agrawal, A.; Milliron, D. J. Influence of Shape on the Surface Plasmon Resonance of Tungsten Bronze Nanocrystals. *Chem. Mater.* **2014**, *26* (5), 1779–1784.
- (21) Momma, K.; Izumi, F. VESTA 3 for Three-Dimensional Visualization of Crystal, Volumetric and Morphology Data. *J. Appl. Crystallogr.* **2011**, 44 (6), 1272–1276.
- (22) Celio, H. Interface Designed with Differential Pumping and Built-in Figure of Merit Method to Monitor Chambers Where Environmentally Sensitive Samples Are Prepared and Transferred for Analysis. 9945761, April 17, 2018.
- (23) Zandi, O.; Agrawal, A.; Shearer, A. B.; Reimnitz, L. C.; Dahlman, C. J.; Staller, C. M.; Milliron, D. J. Impacts of Surface Depletion on the Plasmonic Properties of Doped Semiconductor Nanocrystals. *Nat. Mater.* **2018**, *17* (8), 710–717.
- (24) Chen, L.; Lam, S.; Zeng, Q.; Amal, R.; Yu, A. Effect of Cation Intercalation on the Growth of Hexagonal WO₃ Nanorods. *J. Phys. Chem. C* 2012, 116 (21), 11722–11727.
- (25) Machida, K.; Okada, M.; Adachi, K. Excitations of Free and Localized Electrons at Nearby Energies in Reduced Cesium Tungsten Bronze Nanocrystals. *J. Appl. Phys.* **2019**, *125* (10), 103103.
- (26) Machida, K.; Adachi, K. Ensemble Inhomogeneity of Dielectric Functions in Cs-Doped Tungsten Oxide Nanoparticles. *J. Phys. Chem.* C 2016, 120 (30), 16919–16930.
- (27) Balaji, S.; Djaoued, Y.; Albert, A.-S.; Ferguson, R. Z.; Brüning, R. Hexagonal Tungsten Oxide Based Electrochromic Devices: Spectroscopic Evidence for the Li Ion Occupancy of Four-Coordinated Square Windows. *Chem. Mater.* **2009**, *21* (7), 1381–1389.
- (28) Uppachai, P.; Harnchana, V.; Pimanpang, S.; Amornkitbamrung, V.; Brown, A. P.; Brydson, R. M. D. A Substoichiometric Tungsten Oxide Catalyst Provides a Sustainable

- and Efficient Counter Electrode for Dye-Sensitized Solar Cells. *Electrochim. Acta* **2014**, *145*, 27–33.
- (29) Schaefer, A.; Lefeld, N.; Rahman, M. S.; Gesing, Th. M.; Murshed, M. M. Effects of Air Exposure and Vacuum Storage on Li_{0.4}WO₃ Studied by Photoelectron Spectroscopy. *Appl. Surf. Sci.* **2015**, 357, 608–614.
- (30) Wertheim, G. K.; Campagna, M.; Chazalviel, J.-N.; Buchanan, D. N. E.; Shanks, H. R. Electronic Structure of Tetragonal Tungsten Bronzes and Electrochromic Oxides. *Appl. Phys.* **1977**, *13* (3), 225–230.
- (31) Borgatti, F.; Berger, J. A.; Céolin, D.; Zhou, J. S.; Kas, J. J.; Guzzo, M.; McConville, C. F.; Offi, F.; Panaccione, G.; Regoutz, A.; et al. Revisiting the Origin of Satellites in Core-Level Photoemission of Transparent Conducting Oxides: The Case of n -Doped SnO₂. *Phys. Rev. B* **2018**, *97* (15), 155102.
- (32) Regoutz, A.; Ganose, A. M.; Blumenthal, L.; Schlueter, C.; Lee, T.-L.; Kieslich, G.; Cheetham, A. K.; Kerherve, G.; Huang, Y.-S.; Chen, R.-S.; et al. Insights into the Electronic Structure of OsO₂ Using Soft and Hard x-Ray Photoelectron Spectroscopy in Combination with Density Functional Theory. *Phys. Rev. Mater.* **2019**, 3 (2), 025001.
- (33) Körber, C.; Krishnakumar, V.; Klein, A.; Panaccione, G.; Torelli, P.; Walsh, A.; Da Silva, J. L. F.; Wei, S.-H.; Egdell, R. G.; Payne, D. J. Electronic Structure of In₂O₃ and Sn-Doped In₂O₃ by Hard x-Ray Photoemission Spectroscopy. *Phys. Rev. B* **2010**, *81* (16), 165207.
- (34) Lin, C.; Posadas, A.; Hadamek, T.; Demkov, A. A. Final-State Effect on x-Ray Photoelectron Spectrum of Nominally d¹ and n-Doped d⁰ Transition-Metal Oxides. *Phys. Rev. B* **2015**, *92* (3), 035110.
- (35) Nomoto, J.; Makino, H.; Tsuchiya, T.; Yamamoto, T. Chemical Trends of N-Type Doping of Al, Ga, In, and Ti Donors for ZnO Polycrystalline Films Deposited by Direct-Current Magnetron Sputtering. *J. Appl. Phys.* **2020**, *128* (14), 145303.
- (36) Lu, H.-C.; Katyal, N.; Henkelman, G.; Milliron, D. J. Controlling the Shape Anisotropy of Monoclinic Nb₁₂O₂₉ Nanocrystals Enables Tunable Electrochromic Spectral Range. *J. Am. Chem. Soc.* **2021**, *143*, 19809.
- (37) Chazalviel, J.-N.; Campagna, M.; Wertheim, G. K.; Shanks, H. R. Final-State Effects in the x-Ray Photoelectron Spectra of Cubic Sodium-Tungsten Bronzes. *Phys. Rev. B* **1977**, *16* (2), 697–705.
- (38) Scanlon, D. O.; Watson, G. W.; Payne, D. J.; Atkinson, G. R.; Egdell, R. G.; Law, D. S. L. Theoretical and Experimental Study of the Electronic Structures of MoO₃ and MoO₂. *J. Phys. Chem. C* **2010**, *114* (10), 4636–4645.
- (39) Payne, D. J.; Egdell, R. G.; Hao, W.; Foord, J. S.; Walsh, A.; Watson, G. W. Why Is Lead Dioxide Metallic? *Chem. Phys. Lett.* **2005**, 411 (1), 181–185.
- (40) Gulino, A.; Parker, S.; Jones, F. H.; Egdell, R. G. Influence of Metal–Metal Bonds on Electron Spectra of MoO₂ and WO₂. *J. Chem. Soc. Faraday Trans* **1996**, 92 (12), 2137–2141.
- (41) Tegg, L.; Haberfehlner, G.; Kothleitner, G.; Kisi, E.; Keast, V. J. Crystal Structures, Electrical Properties, and Electron Energy-Loss Spectroscopy of the Sodium and Potassium Tetragonal Tungsten Bronzes. J. Alloys Compd. 2021, 868, 159200.
- (42) Egdell, R. G.; Walker, T. J.; Beamson, G. The Screening Response of a Dilute Electron Gas in Core Level Photoemission from Sb-Doped SnO₂. *J. Electron Spectrosc. Relat. Phenom.* **2003**, *128* (1), 59–66.
- (43) Gibbs, S. L.; Staller, C. M.; Milliron, D. J. Surface Depletion Layers in Plasmonic Metal Oxide Nanocrystals. *Acc. Chem. Res.* **2019**, 52 (9), 2516–2524.
- (44) Franke, M. E.; Koplin, T. J.; Simon, U. Metal and Metal Oxide Nanoparticles in Chemiresistors: Does the Nanoscale Matter? *Small* **2006**, 2 (1), 36–50.
- (45) Payne, D. J.; Paolicelli, G.; Offi, F.; Panaccione, G.; Lacovig, P.; Beamson, G.; Fondacaro, A.; Monaco, G.; Vanko, G.; Egdell, R. G. A Study of Core and Valence Levels in β -PbO $_2$ by Hard X-Ray

Photoemission. J. Electron Spectrosc. Relat. Phenom. 2009, 169 (1), 26–34.

- (46) Xie, F. Y.; Gong, L.; Liu, X.; Tao, Y. T.; Zhang, W. H.; Chen, S. H.; Meng, H.; Chen, J. XPS Studies on Surface Reduction of Tungsten Oxide Nanowire Film by Ar⁺ Bombardment. *J. Electron Spectrosc. Relat. Phenom.* **2012**, *185* (3), 112–118.
- (47) Chun, S. Y.; Park, S.; Lee, S. I.; Nguyen, H. D.; Lee, K.-K.; Hong, S.; Han, C.-H.; Cho, M.; Choi, H.-K.; Kwak, K. Operando Raman and UV-Vis Spectroscopic Investigation of the Coloring and Bleaching Mechanism of Self-Powered Photochromic Devices for Smart Windows. *Nano Energy* **2021**, *82*, 105721.
- (48) Daniel, M. F.; Desbat, B.; Lassegues, J. C.; Gerand, B.; Figlarz, M. Infrared and Raman Study of WO₃ Tungsten Trioxides and WO₃, XH₂O Tungsten Trioxide Hydrates. *J. Solid State Chem.* **1987**, *67* (2), 235–247.
- (49) Okada, M.; Ono, K.; Yoshio, S.; Fukuyama, H.; Adachi, K. Oxygen Vacancies and Pseudo Jahn-Teller Destabilization in Cesium-Doped Hexagonal Tungsten Bronzes. *J. Am. Ceram. Soc.* **2019**, 102 (9), 5386–5400.
- (50) Hibino, M.; Han, W.; Kudo, T. Electrochemical Lithium Intercalation into a Hexagonal WO₃ Framework and Its Structural Change. *Solid State Ion* **2000**, *135* (1), 61–69.
- (51) Han, W.; Hibino, M.; Kudo, T. Hysteresis on the Electrochemical Lithium Insertion and Extraction of Hexagonal Tungsten Trioxide: Influence of Residual Ammonium. *Solid State Ion* **2000**, *128* (1), 25–32.
- (52) Griffith, K. J.; Wiaderek, K. M.; Cibin, G.; Marbella, L. E.; Grey, C. P. Niobium Tungsten Oxides for High-Rate Lithium-Ion Energy Storage. *Nature* **2018**, *559* (7715), *556*–*563*.

□ Recommended by ACS

Size Control of the Mechanism of Exciton Polarization in Metal Oxide Nanocrystals through Fermi Level Pinning

Bharat Tandon and Pavle V. Radovanovic

JULY 12, 2023 ACS NANO

READ 🗹

How to Quantify Electrons in Plasmonic Colloidal Metal Oxide Nanocrystals

Sofia A. Shubert-Zuleta, Delia J. Milliron, et al.

MAY 02, 2023

CHEMISTRY OF MATERIALS

READ 🗹

Dipolar Ligands Tune Plasmonic Properties of Tin-Doped Indium Oxide Nanocrystals

Victor Segui Barragan, Delia J. Milliron, et al.

AUGUST 25, 2023 NANO LETTERS

READ 🗹

Dual-Band Electrochromism in Hydrous Tungsten Oxide

Jenelle Fortunato, Veronica Augustyn, et al.

SEPTEMBER 01, 2023

ACS PHOTONICS

READ 🗹

Get More Suggestions >